ACS APPLIED MATERIALS & INTERFACES

Letter

Prussian Blue Analogue with Fast Kinetics Through Electronic Coupling for Sodium Ion Batteries

Ping Nie, Jiaren Yuan, Jie Wang, Zaiyuan Le, Guiyin Xu, Liang Hao, Gang Pang, Yuting Wu, Hui Dou, Xiaohong Yan, and Xiaogang Zhang

ACS Appl. Mater. Interfaces, **Just Accepted Manuscript** • Publication Date (Web): 01 Jun 2017

Just Accepted

ACS Publications

ACS Applied Materials & Interfaces is published by the American Chemical Society.
1155 Sixteenth Street N.W., Washington, DC 20036

Prussian Blue Analogue with Fast Kinetics Through Electronic Coupling for Sodium Ion Batteries

Ping Nie,[a, †] Jiaren Yuan,[a, †] Jie Wang,[a, †] Zaiyuan Le,[b] Guiyin Xu,[a] Liang Hao,[a] Gang Pang,[a] Yuting Wu,[a] Hui Dou[a], Xiaohong Yan[c] and Xiaogang Zhang[, a]*

[a]Jiangsu Key Laboratory of Materials and Technology for Energy Conversion & College of Material Science and Engineering, Nanjing University of Aeronautics and Astronautics, Nanjing 210016, China.

[b]Department of Chemical and Biomolecular Engineering, University of California, Los Angeles, Los Angeles, California 90095, United States.

[c]School of Material Science and Engineering, Jiangsu University, Zhenjiang 212013, China.

AUTHOR INFORMATION

Corresponding Author

*E-mail: azhangxg@nuaa.edu.cn, azhangxg@163.com

ABSTRACT. Alternative battery systems based on the chemistry of sodium are being considered to offer sustainability and cost-effectiveness. Herein, a simple and new method is demonstrated to enable nickel hexacyanoferrate (NiHCF) Prussian blue analogues (PBA) nanocrystals to be an excellent host for sodium ion storage by functionalization with redox guest molecule. The method is achieved by using NiHCF PBA powders infiltrated with the 7,7,8,8-tetracyanoquinododimethane (TCNQ) solution. Experimental and *ab initio* calculations results suggest that TCNQ molecule bridging with Fe atoms in NiHCF Prussian blue analogue leads to electronic coupling between TCNQ molecules and NiHCF open-framework, which functions as an electrical highway for electron motion and conductivity enhancement. Combining the merits including high electronic conductivity, open framework structure, nanocrystal, and interconnected mesopores, the NiHCF/TCNQ shows high specific capacity, fast kinetics and good cycling stability, delivering a high specific capacity of 35 mAh g^{-1} after 2000 cycles, corresponding a capacity loss of 0.035% decay per cycle.

KEYWORDS. Prussian blue analogue, TCNQ, electronic coupling, sodium ion batteries, fast kinetics

Electrochemical energy storage capable of high energy density and good cycling stability has attracted most attention owing to strong demands for the applications in consumer electronics, electric vehicles, and grid storage.[1-3] The limited resources and greatly increasing demands on available resource of Li pose main concerns with the lithium ion battery (LIB) for large-scale applications. Sodium is naturally abundant, and also exhibits a very suitable redox potential of -2.71 V *vs.* SHE, which is only 0.3 V higher that of metal lithium. Taken together, alternative battery systems based on the chemistry of sodium are being considered to offers sustainability and cost-effectiveness.[4-7] Unfortunately, the ionic radius of Na^+ (1.02 Å) is larger than Li^+ (0.76 Å), which in principle will lead to more sluggish reaction kinetics, and huge volume expansion when sodium ion intercalation into the host materials. The anode materials studies for Na-ion batteries focus on carbonaceous materials,[8-9] Titanium-based intercalation compounds,[10-12] sodium alloys.[13-14] For the positive electrodes in SIBs, alternative electrode materials in particular layered sodium-metal oxides ($NaMnO_2$, Na_xCoO_2, $NaCrO_2$ *etc.*), complex polyanion frameworks including $NaFePO_4$, $Na_3V_2(PO_4)_3$, $Na_4Co_3(PO_4)_2P_2O_7$, and open-framework Prussian blue analogues (PBAs) have been extensively investigated.[15-19] Among them, Prussian blue and its analogues have been investigated as appealing alkali-ion rechargeable battery electrodes, also potential host for various multivalent charge carrier ions because of their open framework structure, large specific area, low cost and simple synthesis.

PBAs have a general formula of $A_xM_1[M_2(CN)_6]_y{\cdot}\square_{1-y}{\cdot}nH_2O$, A: alkaline metal; M_1, M_2: transition metal; and □: $[M_2(CN)_6]$ vacancy. In the crystal structure, transition metal are bound by cyanides to form a face-centered cubic phase. Large interstitial sites within the frameworks can host zeolitic water and guest ions.[20-21] And its open-framework structure enables reversible insertion and rapid transport of a wide variety of alkali cations with very little crystallographic

lattice strain. Alkali-ion intercalation in PBA with fast kinetics in aqueous electrolytes was reported,[18, 20-24] which make PBAs desirable for large energy storage and distributed renewable energy. Importantly, PBAs have been demonstrated as promising host for reversible di-/tri-valent ion insertion, such as Mg^{2+}, Ca^{2+}, Pb^{2+}, Zn^{2+}, Al^{3+}, Y^{3+} in aqueous electrolytes.[25-26] Very recently, Na-rich prussian blue analogues with lower amount of vacancies have been reported by some Labs, which exhibited high Coulombic efficiency and superior capacity retention in Na^+ organic electrolytes.[27-29] Wang and Song *et al.* reported an air stable rhombohedral Prussian white (R-$Na_{1.92}Fe[Fe(CN)_6$) with high Na concentration, which demonstrating a superior performance as cathode materials in sodium ion batteries.[30] High sodium concentration in the structure enables the fabrication of a full cell with non-sodium anode, *e. g*., hard carbon. They further investigated the effect of interstitial H_2O on the structural and sodium storage performance of $Na_{2-\delta}$MnHFC. The dehydrated $Na_{2-\delta}$MnHFC exhibits high potential plateau with high specific capacity of 150 mAh g^{-1}, superior rate capability, and good cycling stability with high capacity retention of 75% for 500 cycles, which is comparable to other reported cathodes in sodium ion batteries.[31] PBAs also have been received great attention as new precursors/templates for preparation of functional nanomaterials with porous structures.[32-33] Our group has recently reported facile preparation of hollow binary metal oxide anodes for LIBs through simple treatment of PBAs in air atmosphere.[34-35] Moreover, Prussian blue analogues has exhibited attractive application for harvesting low-grade thermal energy.[36-37]

One major obstacle for sodium-ion batteries application of the Prussian blue analogues in non-aqueous electrolytes are low Coulombic efficiency and poor cycle stability, associated with low inherent electrical conductivity and structural defects.[28-29, 38] From viewpoint of materials structure, the popularly reported carbon composites strategy is remarkable, which demonstrates

greatly enhanced electric conductivity and cyclability compared with those simply based on bare PBA materials. These carbon components include porous carbon, graphene, carbon nanotubes etc.[39-41] Challenge associated with traditional carbon coating is its difficulty used for PBAs due to its decomposition at high temperature. Therefore, finding an effective strategy to for optimizing the electrochemical properties of PBAs yet having no effects on its open framework characteristic is highly desirable. Herein, we propose a simple and new approach to enable PBAs to be a potential host material for sodium storage by post-synthetic functionalization using 7,7,8,8-tetracyanoquinododimethane (TCNQ) redox molecule. Nickel hexacyanoferrate, one of most promising Prussian blue analogues, is chosen as a demonstration due to its small volume change upon sodium insertion, structural stability and suitable redox potential within the stable electrochemical window of common organic carbonate electrolytes used.[20, 42] As expected, the organic molecule functionalized NiHCF particles exhibits enhanced sodium storage properties with high reversible capacity, fast kinetics, and longest cycling performance compared to other NiHCF based materials reported.

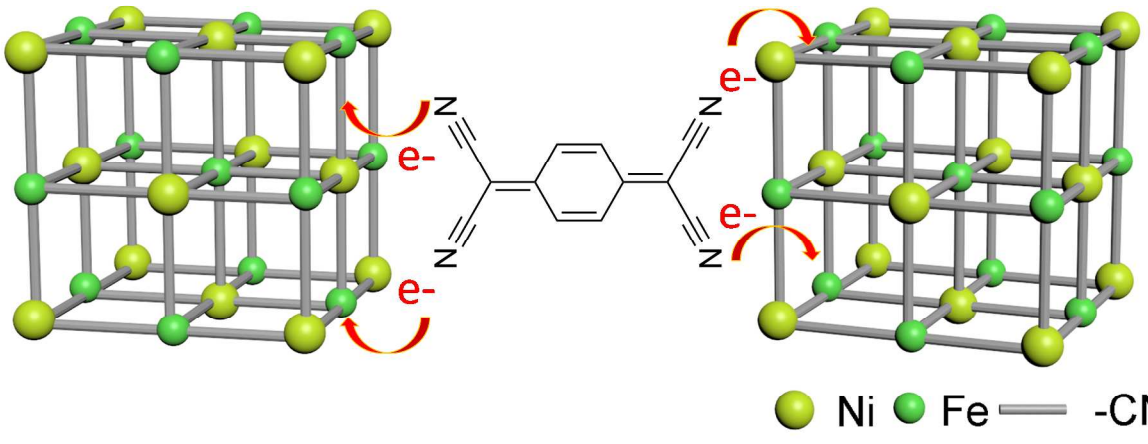

Figure 1. Schematic illustration of the design of nickel hexacyanoferrate conjugated by TCNQ molecule.

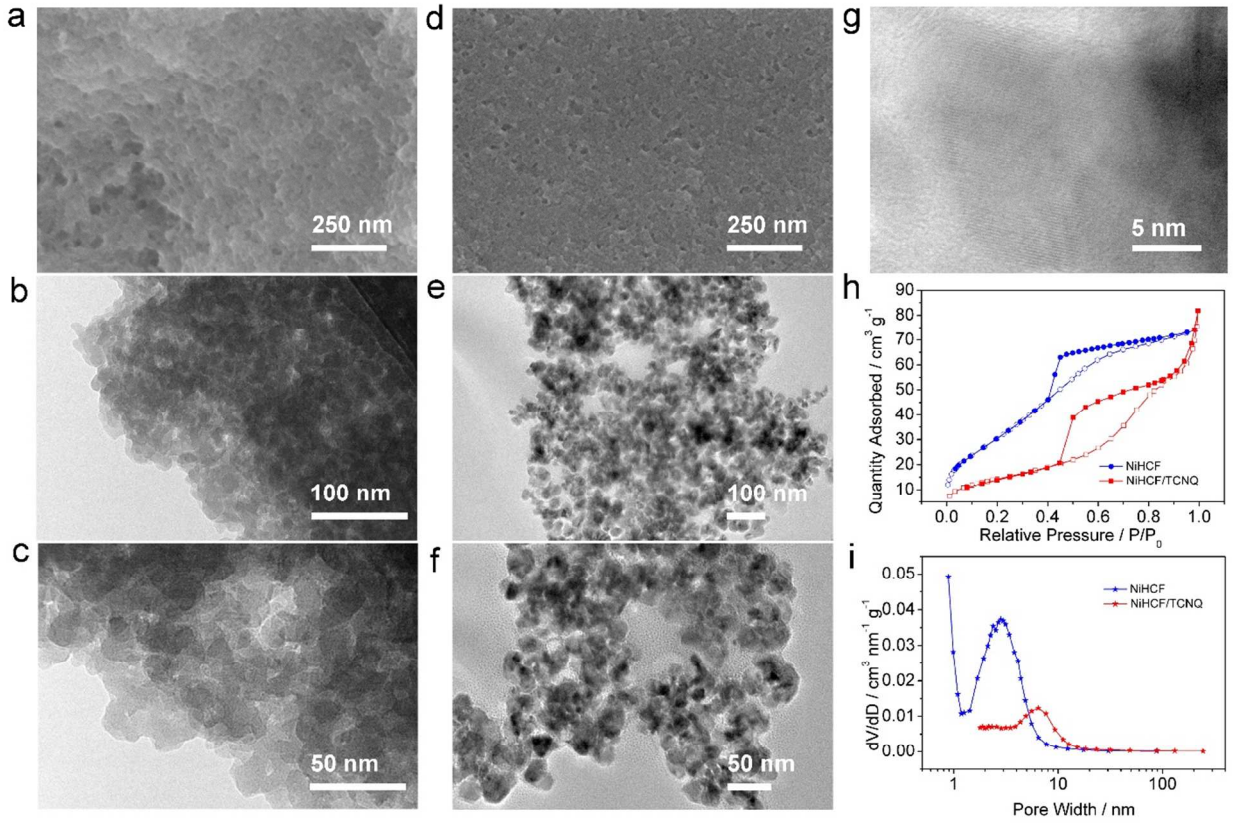

Figure 2. Electron microscope images: SEM and TEM images of NiHCF (a-c) and NiHCF/TCNQ powders (d-f), respectively; g) HRTEM of NiHCF/TCNQ crystal; h and i) N_2 adsorption-desorption isotherms and pore size distribution curves of mesoporous NiHCF and NiHCF/TCNQ samples.

7,7,8,8-tetracyanoquinodimethane organic molecule has been demonstrated one of the strongest organic electron acceptors, which possess higher electron affinity of 3.22 eV due to its planar structure and four cyano groups. All P electrons of N and C atoms participate in the formation of P-π conjugation.[43-44] Due to its higher electron affinity, TCNQ could combine with metal species of nickel hexacyanoferrate PBAs (Fe: $[Ar]4s^23d^6$, Ni: $[Ar]4s^23d^8$) and create a

unique opportunity for electrical conductivity enhancement (**Figure 1**). Mesoporous nickel hexacyanoferrate (NiHCF) was first synthesized through simple co-precipitation as described in a recent reported paper.[42] After vacuum drying, the NiHCF powers were immersed into a saturated TCNQ/dichloromethane solution for certain time, followed by naturally removing the dichloromethane under ambient temperature.

The microstructure of the two samples is imaged by FESEM and TEM (**Figure 2**). The SEM image shows that the continuous networks of highly mesoporous NiHCF powers with small particle size. There is no obvious difference in morphology after TCNQ decoration (**Figure 2**d). The observations in the SEM images are also supported by TEM results (**Figure 2**b, c). As shown in **Figure 2**e, f, when the NiHCF was infiltrated with TCNQ solution, the resulting product shows similar nanocrystal morphology. Obvious lattice fringes in HRTEM image confirmed its crystalline characteristic (**Figure 2**g). The porous structure of the NiHCF is further investigated by nitrogen sorption isotherms, as shown in **Figure 2**h, i. The particles possess a specific surface area of 129.1 m^2 g^{-1}, and the pore sizes mainly range from 2-10 nm. It is believed that the interconnected mesopores would enhance the contact between electrode/electrolyte and shorten sodium ion diffusion distance, facilitating fast charge transfer reactions in battery operation. The NiHCF/TCNQ composite presents a smaller specific surface area of 52.3 m^2 g^{-1} with pore size distribution mainly in the region of *ca.* 3-20 nm. The decrease in specific surface could be contributed to the infiltration with TCNQ saturated solution, where the TCNQ filled into the voids and pores of NiHCF material and/or coated on its surface after drying, causing a significant loss in surface area. Furthermore, this result is also confirmed by the decreasing microspores in pore size distribution curves in **Figure 2**i, while the mesopores still remain in NiHCF/TCNQ. The composition of NiHCF was also further characterized by

thermogravimetric analysis (TGA) (**Figure S1**). The initial mass loss of 21.3 wt.% at around 250 □ can be assigned to the evaporation of weakly bonded and coordinated water molecules, which is very similar to the results reported in the literature.[45] As can be seen in **Figure S1**b, the mass loss trends for the two materials are similar. For the NiHCF/TCNQ composite, the first step mass loss of 19.9% below 260 □ also corresponds to the evaporation of moisture and coordinated water molecules. And further mass loss of 11.2% at 260-550 □ is addressed to the decomposition of the composite.

As shown in **Figure 3**a, NiHCF/TCNQ composites show similar Powder XRD patterns to pristine NiHCF sample, which can be indexed to the face-centered cubic structure, confirming that the PBA crystalline structure was not affected by the TCNQ infiltration process. Significant XRD diffraction peak broadening indicates the small crystal size of NiHCF. The calculated crystallite size was estimated to be ~8.75 nm based on (200) plane according to Scherrer equation:

$$D_p = \frac{0.94\lambda}{\beta_{1/2}\cos\theta} \quad (1)$$

where D_p is average crystallite size, β corresponds to line broadening in radians (FWHM), θ is Bragg angle, λ is X-ray wavelength (0.154056 nm), being consistent with the electron microscope analysis above. In addition, low diffraction peaks of TCNQ can be observed (marked by diamond in **Figure 3**a, for comparison, XRD pattern of pristine TCNQ molecule is shown in **Figure 3**b), indicating the some TCNQ molecule resides on the surface of NiHCF structure. Ultraviolet-visible spectroscopy was recorded from pure NiHCF, NiHCF/TCNQ composite, and TCNQ molecule. An absorption peak at around 410 nm in NiHCF/TCNQ corresponds to neutral

TCNQ molecule. The peak centered at 300 nm in NiHCF shifts to 330 nm in NiHCF/TCNQ is a well-known signature for charge transfer, demonstrating partial charge transfer between NiHCF

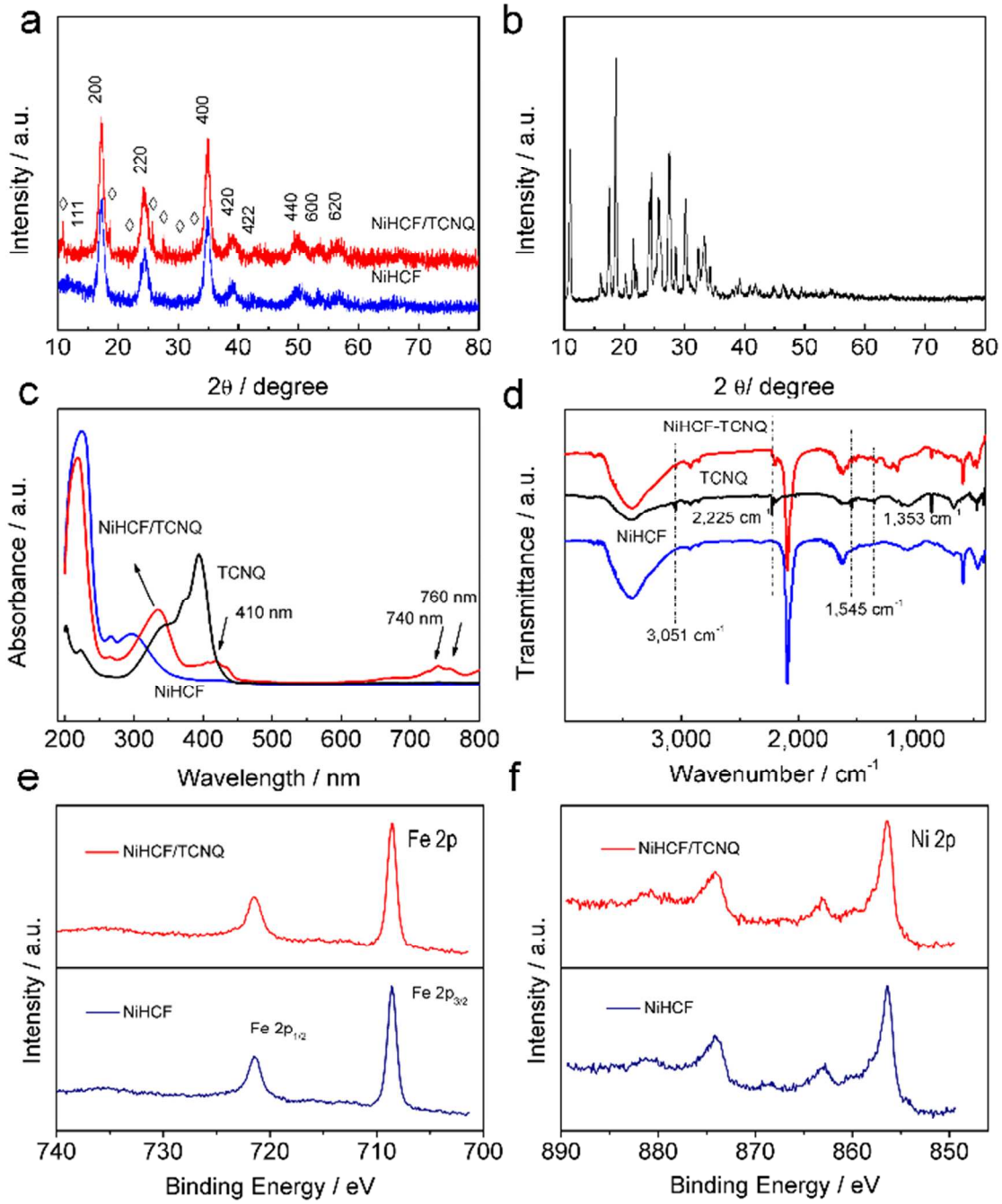

Figure 3. Structural information of TCNQ, NiHCF, and NiHCF/TCNQ *via* XRD, Transmission UV-vis spectra, Infrared spectra, and XPS: a) XRD patterns of NiHCF and NiHCF/TCNQ; b)

XRD pattern of TCNQ molecule; c) UV-vis spectra, d) Infrared spectra and e, f) Fe 2p and Ni 2p XPS spectra of NiHCF, and NiHCF/TCNQ samples, respectively.

framework and TCNQ molecule. By using Fourier transform infrared (FTIR) analysis, new absorption peaks at 3051, 2225, 1545, 1353 cm^{-1} from TCNQ molecule are observed in NiHCF/TCNQ composite after infiltration with TCNQ. Furthermore, the NiHCF/TCNQ shows the bands of stretching vibrations from *v*(O-H) in water molecule (3425 cm^{-1}), CN^- (2094 cm^{-1}), stretching mode of OH (1620 cm^{-1}), which are characteristic absorption peaks of NiHCF PBAs. The local atomic environment of Fe, Ni in the NiHCF/TCNQ composites after TCNQ infiltration was further analyzed using X-ray photoelectron spectroscopy (XPS) technology. Fe, Ni in NiHCF remain the same state after infiltration process, as revealed by XPS (**Figure 3**e, f, **Figure S2**).

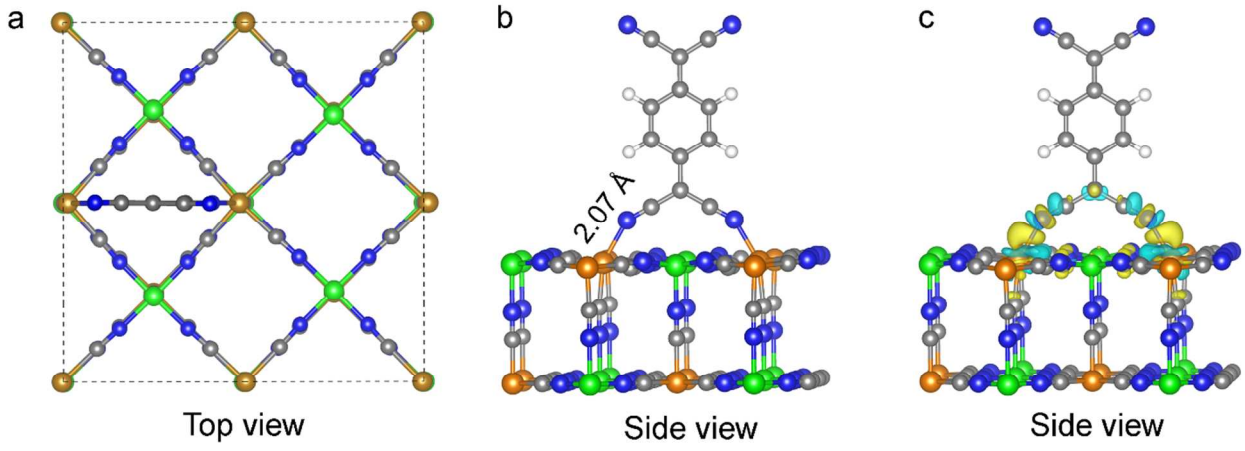

Figure 4. Density functional theory (DFT) analysis of interaction mechanism of TCNQ molecule and NiHCF PBAs: (a, b) optimized geometric configurations for TCNQ on NiHCF surface, (c) the charge difference density for TCNQ functionalized NiHCF PBA. The blue isosurface corresponds electron depletion zones while the yellow one denotes electron accumulation zones.

To better reveal the effect of TCNQ functionalization, the guest-host interaction mechanism of TCNQ molecule and metal Fe/Ni in NiHCF open-framework is further studied by DFT calculations. As displayed in **Figure 4**a, b, the calculations show that TCNQ molecule is adsorbed on the surface of metal Fe/Ni in NiHCF open-framework. The molecule binds well on the host surface by two Fe-N bonds with a bond length of about 2.07 Å. The binding energy (E_b) is calculated to be 0.04 eV. The interaction originates from hybridization between N and Fe atom which can be analyzed from charge difference density (**Figure 4**c). The electrons accumulated between N and Fe atom enable moderate coupling between the PBA and TCNQ, which is similar to strong electronic coupling between the MOF $Cu_3(BTC)_2$ and TCNQ molecule.[46] And the charge transfer could also be supported by UV-vis spectra discussed above. Based on the DFT calculation results, it is reasonable to assume that the interaction not only renders the TCNQ molecule promising for application as a link to connect NiHCF nanoparticles, but offers effective route for tuning the density of carriers in Fe/Ni in NiHCF open-framework, finally forming an electrical highway for electron motion and conductivity enhancement. Wang *et al.* reported enhanced electrochemical performance of $LiFePO_4$ by molecular charge transport layers.[47] Their findings demonstrate that a single molecular layer of 4-[bis (4-methoxyphenyl) amino] benzylphosphonic acid (BMABP) single molecule layer facilitates desired electronic charge transport and meanwhile allowing fast Li^+ exchange across the solid/electrolyte interface. Experiment results demonstrated that surface bound molecular relays afford electrochemical reaction of $LiFePO_4$ cathode with low electronic conductivity. This new design not only could reduce the amount of conductive additive to increase substantially energy density, but opening up the possibility to enhance electrode rate capability.

We further evaluated the electrochemical properties of the two NiHCF and NiHCF/TCNQ as cathodes for sodium ion batteries by using half-cells. **Figure 5**a shows the initial four cycling cyclic voltammetry curves of the NiHCF/TCNQ composite at a scan rate of 0.1 mV s^{-1}, which exhibit sharper redox peaks when compared with the pristine NiHCF electrode (**Figure S3**). The potential separation between oxidation and reduction peaks is smaller than the untreated sample, demonstrating lower overall resistance and better kinetics characteristics of the redox reaction. Furthermore, an additional peak at around 2.2 V from TCNQ molecule can also be observed (**Figure S5**a, b).

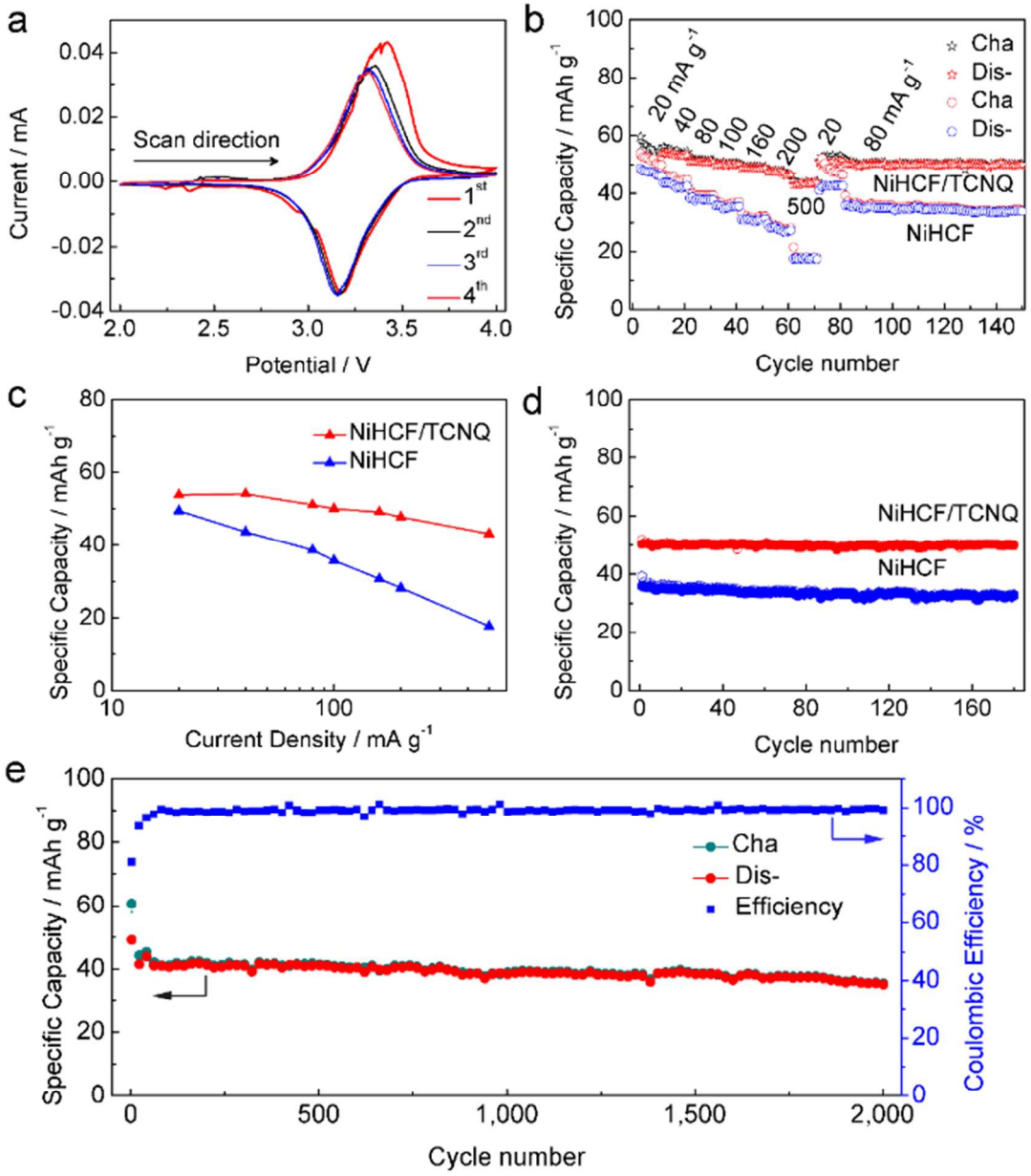

Figure 5. Electrochemical performance: a) cyclic voltammograms for NiHCF/TCNQ at a sweep rate of 0.1 mV s^{-1}; b, c) rate performance of NiHCF and NiHCF/TCNQ at various current densities from 20 to 500 mA g^{-1}; d) extended cycling performance after C-rate cycles in Figure b; e) long-term cycle retention and Coulombic efficiency of the NiHCF/TCNQ electrode at a current density of 80 mA g^{-1}.

As expected, the composite shows higher specific capacity than the control sample (56.4 mAh g^{-1} *vs.* 49.5 mAh g^{-1}) from the galvanostatically potential profiles (**Figure S4**). In order to evaluate the effect of TCNQ molecule to electrochemical properties of NiHCF PBAs, the sodium storage properties of TCNQ molecule were also tested under the same condition in the potential range of 2.0-4.0 V. As exhibited in **Figure S5**, the TCNQ exhibit obvious electrochemical activity in the same potential range when operating in a 1 M $NaClO_4$/EC-PC electrolyte. However, the material shows dramatic capacity fading within the cycles. The initial specific capacity is around 25 mAh g^{-1}, but it fades to 2.9 mAh g^{-1} after 5 cycles, which is consistent with CV test results. The capacity contribution is almost negligible after 10 cycles (1.7 mAh g^{-1}, **Figure S5**d), revealing that the TCNQ molecule has insignificant capacity contribution to the electrochemical performance of the resulting NiHCF electrode.

The rate performance of the two electrodes are shown in **Figure 5**b. The NiHCF/TCNQ composite shows higher capacity at various current rate from 20 to 500 mA g^{-1} as compared with the control samples. A specific capacity of 56.4, 54.2, 51.2, 49.8, 48.9, 47.6 mAh g^{-1} can be delivered at the current density of 20, 40, 80, 100, 160, 200 mA g^{-1}, respectively. Even at higher rate of 500 mA g^{-1}, high capacity of 43 mAh g^{-1} can be achieved, indicating high reversible charge/discharge over a wide range of operating current rate. When the current was recovered to 20 mA g^{-1} after high current density cycling, the specific capacity of the NiHCF/TCNQ electrode reverts to the initial value, indicating good reversibility. By contrast, the capacity is lower for pristine NiHCF electrode at the same range of current densities. The specific capacity is 49.5 mA h g^{-1} at the first discharge at 20 mA g^{-1}, then subsequently drops to 29.4 mA h g^{-1} with an increasing current density to 0.2 A g^{-1}. The specific capacity can be recovered to 41 mA h g^{-1} if tested again under low rate of 20 mA g^{-1}. A comparison of the rate capabilities for the two

materials is shown in **Figure 5**c, the composite exhibits a significant improvement of rate performance when current density is varied from 20 to 500 mA g^{-1}. Furthermore, the NiHCF/TCNQ shows decent cyclability when cycling at a current rate of 80 mAh g^{-1}, more than 99.2 % capacity is maintained after 180 cycles (**Figure 5**d). The capacity of the composite is larger than that of pristine materials during the cycling. After 2000 cycles at a current rate of 80 mAh g^{-1}, the capacity still remains at 35 mAh g^{-1} without obvious decay, nearly with only 0.035% decay per cycle (**Figure 5**e). The results are comparable to the works related to NiHCF electrode reported in the literature (**Table S1**), including mesoporous NiHCF and NiHCF nanoparticles.[42, 45] The above electrochemical results have demonstrated the superior rate performance and good cycling stability of NiHCF/TCNQ electrode for advanced sodium-ion batteries.

The impressive electrochemical properties can be attributed to the following aspects. Specifically, improved conductivity arising from TCNQ molecule bridging the Fe atoms in the framework function as the electrical highway for electron transfer, playing an important role in promoting fast kinetics of Na^+ insertion/extraction, and hence improving the electrochemical properties of NiHCF, which was further confirmed by the electrochemical impedance spectroscopy (EIS) of NiHCF and NiHCF/TCNQ as described in **Figure S6**. The frequency range was performed between 100 kHz to 0.01 Hz with a signal amplitude of 5 mV. The impedance spectra consist of a depressed semicircle in the high frequency region attributed to the charge-transfer resistance (R_{ct}), and an inclined line at low frequency, corresponding to the di□usion of lithium ions in the active materials, respectively.[48-49] The NiHCF/TCNQ electrode presents relatively low charge-transfer resistance than that of the pristine NiHCF electrodes, and thus indicating more fast kinetics for upon the sodiation/desodiation. The Nyquist plots are

further modelled and fitted. The calculated R_{ct} extracted from the high-frequency range was 1254 and 631 Ω for the bare NiHCF and NiHCF/TCNQ electrode, respectively. On the other hand, nanocrystal morphology of NiHCF Prussian blue analogues has a more favorable electron diffusion dimension and reduced migration barrier for Na^+ ion. Moreover, the well-designed mesoporous structure increases the contact area for electrolytes, allowing facile intercalation and diffusion of Na^+. Lastly, the open-framework structure could maintain structural integrity while sodium ions are accommodated, resulting in good structural robustness for stable cycling.

In summary, we have developed a simple and novel strategy to enable PBAs with good cycling and ultrahigh rate performance for sodium ion storage through post-synthetic functionalization using 7,7,8,8-tetracyanoquinododimethane (TCNQ) guest molecule. Experimental and *ab initio* calculations results revealed that TCNQ molecule bridging with Fe atoms in NiHCF Prussian blue analogues leads to electronic coupling between these molecules and NiHCF open-framework, which can function as an electrical highway for electron motion and conductivity enhancement. The obtained NiHCF/TCNQ showed high rate capability and maintained a high specific capacity of 35 mAh g^{-1} after 2000 cycles, corresponding a capacity loss of 0.035% decay per cycle. We expect that these initial studies on the fundamental organic functionalization of Prussian blue analogue will provide access to unprecedented novel materials for the development of high-performance energy storage and conversion devices.

ASSOCIATED CONTENT

Supporting Information. Experimental section, computational methods, TGA curves, XPS spectra, cyclic voltammograms, charge-discharge curves, electrochemical properties of the 7,7,8,8-tetracyanoquinododimethane, Nyquist plots.

AUTHOR INFORMATION

Corresponding Author

*E-mail: azhangxg@nuaa.edu.cn

Notes

† These authors contributed equally to this work. The authors declare no competing financial interest.

ACKNOWLEDGMENT

We gratefully ackonwledage financial support from the National Program on Key Basic Research Project of China (no. 2014CB239701), National Natural Science Foundation of China (nos. 51372116, 51672128), Prospective Joint Research Project of Cooperative Innovation Fund of Jiangsu Province(BY2015003-7), Anhui Provincial Natural Science Foundation (nos. KJ2016A092, 1708085QE115), Project Funded by the Priority Academic Program Development of Jiangsu Higher Education Institutions (PAPD) and the support of computer resources from National Supercomputing Center in Shenzhen. P. Nie acknowledges Funding for Outstanding Doctoral Dissertation in NUAA (no. BCXJ14-12), Funding of Jiangsu Innovation Program for Graduate Education (no. KYLX_0254, KYZZ16_0166), and China Scholarship Council (no. 201406830023) for providing a scholarship for studying at University of California, Los Angeles as a visiting graduate. Y. Wu acknowledges Founding of Graduate Innovation Center in NUAA (no. kfjj20160601).

REFERENCES

(1) Armand, M.; Tarascon, J. M. Building Better Batteries. *Nature* **2008,** *451*, 652-657.
(2) Dunn, B.; Kamath, H.; Tarascon, J.-M., Electrical Energy Storage for the Grid: A Battery of Choices. *Science* **2011,** *334*, 928-935.
(3) Chen, Z.; Peng, Y. T.; Liu, F.; Le, Z. Y.; Zhu, J.; Shen, G. R.; Zhang, D. Q.; Wen, M. C.; Xiao, S. N.; Liu, C. P.; Lu, Y. F.; Li, H. X. Hierarchical Nanostructured WO_3 with Biomimetic Proton Channels and Mixed Ionic-Electronic Conductivity for Electrochemical Energy Storage. *Nano Lett.* **2015,** *15*, 6802-6808.
(4) Kundu, D.; Talaie, E.; Duffort, V.; Nazar, L. F. The Emerging Chemistry of Sodium Ion Batteries for Electrochemical Energy Storage. *Angew. Chem., Int. Ed.* **2015,** *54*, 3431-3448.
(5) Palomares, V.; Serras, P.; Villaluenga, I.; Hueso, K. B.; Carretero-Gonzalez, J.; Rojo, T. Na-ion Batteries, Recent Advances and Present Challenges to Become Low Cost Energy Storage Systems. *Energy Environ. Sci.* **2012,** *5*, 5884-5901.
(6) Chen, Z.; Augustyn, V.; Jia, X.; Xiao, Q.; Dunn, B.; Lu, Y. High-Performance Sodium-Ion Pseudocapacitors Based on Hierarchically Porous Nanowire Composites. *ACS Nano* **2012,** *6*, 4319-4327.
(7) Le, Z.; Liu, F.; Nie, P.; Li, X.; Liu, X.; Bian, Z.; Chen, G.; Wu, H. B.; Lu, Y. Pseudocapacitive Sodium Storage in Mesoporous Single-Crystal-like TiO_2–Graphene Nanocomposite Enables High-Performance Sodium-Ion Capacitors. *ACS Nano* **2017,** *11*, 2952-2960.
(8) Stevens, D. A.; Dahn, J. R. High Capacity Anode Materials for Rechargeable Sodium - Ion Batteries. *J. Electrochem. Soc.* **2000,** *147*, 1271-1273.
(9) Bommier, C.; Ji, X. Recent Development on Anodes for Na-Ion Batteries. *Isr. J. Chem.* **2015,** *55*, 486-507.
(10) Zhao, L.; Pan, H.-L.; Hu, Y.-S.; Li, H.; Chen, L.-Q. Spinel Lithium Titanate ($Li_4Ti_5O_{12}$) as Novel Anode Material for Room-Temperature Sodium-Ion Battery. *Chin. Phys. B* **2012,** *21*, 028201.
(11) Wang, Y.; Yu, X.; Xu, S.; Bai, J.; Xiao, R.; Hu, Y.-S.; Li, H.; Yang, X.-Q.; Chen, L.; Huang, X. A Zero-Strain Layered Metal Oxide as the Negative Electrode for Long-Life Sodium-Ion Batteries. *Nat. Commun.* **2013,** *4*, 2365.
(12) Senguttuvan, P.; Rousse, G.; Seznec, V.; Tarascon, J.-M.; Palacín, M. R. $Na_2Ti_3O_7$: Lowest Voltage Ever Reported Oxide Insertion Electrode for Sodium Ion Batteries. *Chem. Mater.* **2011,** *23*, 4109-4111.
(13) Li, Z.; Ding, J.; Mitlin, D. Tin and Tin Compounds for Sodium Ion Battery Anodes: Phase Transformations and Performance. *Acc. Chem. Res.* **2015,** *48*, 1657-1665.
(14) Liu, J.; Wen, Y.; van Aken, P. A.; Maier, J.; Yu, Y. Facile Synthesis of Highly Porous Ni–Sn Intermetallic Microcages with Excellent Electrochemical Performance for Lithium and Sodium Storage. *Nano Lett.* **2014,** *14*, 6387-6392.
(15) Braconnier, J.-J.; Delmas, C.; Fouassier, C.; Hagenmuller, P. Comportement Electrochimique Des Phases Na_xCoO_2. *Mater. Res. Bull.* **1980,** *15*, 1797-1804.
(16) Komaba, S.; Takei, C.; Nakayama, T.; Ogata, A.; Yabuuchi, N. Electrochemical Intercalation Activity of Layered $NaCrO_2$ *vs.* $LiCrO_2$. *Electrochem. Commun.* **2010,** *12*, 355-358.
(17) Zhu, C.; Song, K.; van Aken, P. A.; Maier, J.; Yu, Y. Carbon-Coated $Na_3V_2(PO_4)_3$ Embedded in Porous Carbon Matrix: An Ultrafast Na-Storage Cathode with the Potential of Outperforming Li Cathodes. *Nano Lett.* **2014,** *14*, 2175-2180.

(18) Lu, Y.; Wang, L.; Cheng, J.; Goodenough, J. B. Prussian Blue: a New Framework of Electrode Materials for Sodium Batteries. *Chem. Commun.* **2012,** *48*, 6544-6546.
(19) Xiang, X.; Zhang, K.; Chen, J. Recent Advances and Prospects of Cathode Materials for Sodium-Ion Batteries. *Adv. Mater.* **2015,** *27*, 5343-5364.
(20) Wessells, C. D.; Peddada, S. V.; Huggins, R. A.; Cui, Y. Nickel Hexacyanoferrate Nanoparticle Electrodes For Aqueous Sodium and Potassium Ion Batteries. *Nano Lett.* **2011,** *11*, 5421-5425.
(21) Wessells, C. D.; Huggins, R. A.; Cui, Y. Copper Hexacyanoferrate Battery Electrodes with Long Cycle Life and High Power. *Nat. Commun.* **2011,** *2*, 550.
(22) Wang, L.; Lu, Y.; Liu, J.; Xu, M.; Cheng, J.; Zhang, D.; Goodenough, J. B. A Superior Low-Cost Cathode for a Na-Ion Battery. *Angew. Chem., Int. Ed.* **2013,** *52*, 1964-1967.
(23) Nie, P.; Shen, L.; Luo, H.; Ding, B.; Xu, G.; Wang, J.; Zhang, X. Prussian Blue Analogues: a New Class of Anode Materials for Lithium Ion Batteries. *J. Mater. Chem. A* **2014,** *2*, 5852-5857.
(24) Nie, P.; Shen, L.; Pang, G.; Zhu, Y.; Xu, G.; Qing, Y.; Dou, H.; Zhang, X. Flexible Metal-Organic Frameworks as Superior Cathodes for Rechargeable Sodium-Ion Batteries. *J. Mater. Chem. A* **2015,** *3*, 16590-16597.
(25) Wang, R. Y.; Shyam, B.; Stone, K. H.; Weker, J. N.; Pasta, M.; Lee, H.-W.; Toney, M. F.; Cui, Y. Reversible Multivalent (Monovalent, Divalent, Trivalent) Ion Insertion in Open Framework Materials. *Adv. Energy Mater.* **2015,** *5*, 1401869.
(26) Li, Z.; Xiang, K.; Xing, W.; Carter, W. C.; Chiang, Y.-M. Reversible Aluminum-Ion Intercalation in Prussian Blue Analogs and Demonstration of a High-Power Aluminum-Ion Asymmetric Capacitor. *Adv. Energy Mater.* **2015,** *5*, 201401410.
(27) You, Y.; Yu, X.; Yin, Y.; Nam, K.-W.; Guo, Y.-G. Sodium Iron Hexacyanoferrate with High Na Content as a Na-Rich Cathode Material for Na-Ion Batteries. *Nano Res.* **2015,** *8*, 117-128.
(28) Liu, Y.; Qiao, Y.; Zhang, W.; Li, Z.; Ji, X.; Miao, L.; Yuan, L.; Hu, X.; Huang, Y. Sodium Storage in Na-rich $Na_xFeFe(CN)_6$ Nanocubes. *Nano Energy* **2015,** *12*, 386-393.
(29) Li, W.-J.; Chou, S.-L.; Wang, J.-Z.; Kang, Y.-M.; Wang, J.-L.; Liu, Y.; Gu, Q.-F.; Liu, H.-K.; Dou, S.-X. Facile Method To Synthesize Na-Enriched $Na_{1+x}FeFe(CN)_6$ Frameworks as Cathode with Superior Electrochemical Performance for Sodium-Ion Batteries. *Chem. Mater.* **2015,** *27*, 1997-2003.
(30) Wang, L.; Song, J.; Qiao, R.; Wray, L. A.; Hossain, M. A.; Chuang, Y.-D.; Yang, W.; Lu, Y.; Evans, D.; Lee, J.-J.; Vail, S.; Zhao, X.; Nishijima, M.; Kakimoto, S.; Goodenough, J. B. Rhombohedral Prussian White as Cathode for Rechargeable Sodium-Ion Batteries. *J. Am. Chem. Soc.* **2015,** *137*, 2548-2554.
(31) Song, J.; Wang, L.; Lu, Y.; Liu, J.; Guo, B.; Xiao, P.; Lee, J.-J.; Yang, X.-Q.; Henkelman, G.; Goodenough, J. B. Removal of Interstitial H_2O in Hexacyanometallates for a Superior Cathode of a Sodium-Ion Battery. *J. Am. Chem. Soc.* **2015,** *137*, 2658-2664.
(32) Hu, M.; Ishihara, S.; Yamauchi, Y. Bottom-Up Synthesis of Monodispersed Single-Crystalline Cyano-Bridged Coordination Polymer Nanoflakes. *Angew. Chem. Int. Ed.* **2013,** *52*, 1235-1239.
(33) Yu, X.-Y.; Yu, L.; Wu, H. B.; Lou, X. W. Formation of Nickel Sulfide Nanoframes from Metal–Organic Frameworks with Enhanced Pseudocapacitive and Electrocatalytic Properties. *Angew. Chem. Int. Ed.* **2015,** *54*, 5331-5335.

(34) Nie, P.; Shen, L.; Luo, H.; Li, H.; Xu, G.; Zhang, X. Synthesis of Nanostructured Materials by Using Metal-Cyanide Coordination Polymers and Their Lithium Storage Properties. *Nanoscale* **2013,** *5*, 11087-11093.
(35) Hou, L.; Lian, L.; Zhang, L.; Pang, G.; Yuan, C.; Zhang, X. Self-Sacrifice Template Fabrication of Hierarchical Mesoporous Bi-Component-Active ZnO/$ZnFe_2O_4$ Sub-Microcubes as Superior Anode Towards High-Performance Lithium-Ion Battery. *Adv. Funct. Mater.* **2015,** *25*, 238-246.
(36) Lee, S. W.; Yang, Y.; Lee, H.-W.; Ghasemi, H.; Kraemer, D.; Chen, G.; Cui, Y. An Electrochemical System for Efficiently Harvesting Low-Grade Heat Energy. *Nat. Commun.* **2014,** *5*, 3942.
(37) Yang, Y.; Lee, S. W.; Ghasemi, H.; Loomis, J.; Li, X.; Kraemer, D.; Zheng, G.; Cui, Y.; Chen, G. Charging-Free Electrochemical System for Harvesting Low-Grade Thermal Energy. *Proc. Natl. Acad. Sci.* **2014,** *111*, 17011-17016.
(38) Wu, X.; Deng, W.; Qian, J.; Cao, Y.; Ai, X.; Yang, H. Single-Crystal $FeFe(CN)_6$ Nanoparticles: a High Capacity and High Rate Cathode for Na-Ion Batteries. *J. Mater. Chem. A* **2013,** *1*, 10130-10134.
(39) Jiang, Y.; Yu, S.; Wang, B.; Li, Y.; Sun, W.; Lu, Y.; Yan, M.; Song, B.; Dou, S. Prussian Blue@C Composite as an Ultrahigh-Rate and Long-Life Sodium-Ion Battery Cathode. *Adv. Funct. Mater.* **2016,** *26*, 5315-5321.
(40) You, Y.; Yao, H.-R.; Xin, S.; Yin, Y.-X.; Zuo, T.-T.; Yang, C.-P.; Guo, Y.-G.; Cui, Y.; Wan, L.-J.; Goodenough, J. B. Subzero-Temperature Cathode for a Sodium-Ion Battery. *Adv. Mater.* **2016,** *28*, 7243-7248.
(41) Zhang, M.; Hou, C.; Halder, A.; Ulstrup, J.; Chi, Q. Interlocked Graphene–Prussian Blue Hybrid Composites Enable Multifunctional Electrochemical Applications. *Biosens. Bioelectron.* **2017,** *89,* 570-577.
(42) Yue, Y.; Binder, A. J.; Guo, B.; Zhang, Z.; Qiao, Z.-A.; Tian, C.; Dai, S. Mesoporous Prussian Blue Analogues: Template-Free Synthesis and Sodium-Ion Battery Applications. *Angew. Chem., Int. Ed.* **2014,** *53*, 3134-3137.
(43) Ma, L.; Hu, P.; Kloc, C.; Sun, H.; Michel-Beyerle, M. E.; Gurzadyan, G. G. Ultrafast Spectroscopic Characterization of 7,7,8,8-Tetracyanoquinodimethane (TCNQ) and Its Radical Anion (TCNQ−). *Chem. Phys. Lett.* **2014,** *609*, 11-14.
(44) Jiang, W.; Zhang, M.; Wang, J.; Liu, Y.; Zhu, Y. Dramatic Visible Activity in Phenol Degradation of TCNQ@TiO_2 Photocatalyst With Core–Shell Structure. *Appl. Catal., B* **2014,** *160–161*, 44-50.
(45) You, Y.; Wu, X.-L.; Yin, Y.-X.; Guo, Y.-G. A Zero-Strain Insertion Cathode Material of Nickel Ferricyanide for Sodium-Ion Batteries. *J. Mater. Chem. A* **2013,** *1*, 14061-14065.
(46) Talin, A. A.; Centrone, A.; Ford, A. C.; Foster, M. E.; Stavila, V.; Haney, P.; Kinney, R. A.; Szalai, V.; El Gabaly, F.; Yoon, H. P.; Léonard, F.; Allendorf, M. D. Tunable Electrical Conductivity in Metal-Organic Framework Thin-Film Devices. *Science* **2014,** *343*, 66-69.
(47) Wang, Q.; Evans, N.; Zakeeruddin, S. M.; Exnar, I.; Grätzel, M. Molecular Wiring of Insulators: Charging and Discharging Electrode Materials for High-Energy Lithium-Ion Batteries by Molecular Charge Transport Layers. *J. Am. Chem. Soc.* **2007,** *129*, 3163-3167.
(48) Peng, Y.; Le, Z.; Wen, M.; Zhang, D.; Chen, Z.; Wu, H. B.; Li, H.; Lu, Y. Mesoporous Single-Crystal-Like TiO_2 Mesocages Threaded With Carbon Nanotubes for High-Performance Electrochemical Energy Storage. *Nano Energy* **2017,** *35*, 44-51.

(49) Nie, P.; Liu, X.; Fu, R.; Wu, Y.; Jiang, J.; Dou, H.; Zhang, X. Mesoporous Silicon Anodes by Using Polybenzimidazole Derived Pyrrolic N-Enriched Carbon toward High-Energy Li-Ion Batteries. *ACS Energy Lett.* **2017**, 1279-1287.

Table of Contents Graphic